PAPER

Check for updates

Experimental and theoretical evidence for low-lying excited states in [Cr$_6$E$_8$(PEt$_3$)$_6$] (E = S, Se, Te) cluster molecules†

Patrick Bügel, [iD] [a] Ivo Krummenacher,[b] Florian Weigend [iD] [c] and
Andreas Eichhöfer [iD] *[a,d]

Three [Cr$_6$E$_8$(PEt$_3$)$_6$] cluster molecules with E = S, Se, and Te have been synthesized by reaction of stoichiometric mixtures of Cr(II) and Cr(III) metal salts with silylated chalcogen reagents E(SiMe$_3$)$_2$ (E = S, Se, Te) in the presence of L = PEt$_3$ = triethylphosphine. For the sulfide- and selenide-bridged clusters two crystallographic forms (trigonal $R\bar{3}$ and triclinic $P\bar{1}$), which differ in the presence of lattice solvent molecules, have been isolated. Structural data, optical spectra and quantum chemical calculations reveal the presence of low-lying excited states in [Cr$_6$E$_8$(PEt$_3$)$_6$] (E = S, Se), which would help in rationalizing the non-vanishing magnetic moments at 2 K revealed by DC magnetic measurements and EPR spectroscopy. These findings are partially in contrast to a previous report by Saito and co-workers (S. Kamiguchi, H. Imoto, T. Saito, *Inorg. Chem.*, 1998, **37**, 6852–6857.), who postulated an incorporated hydrogen atom as the source of paramagnetism at low temperatures for the trigonal forms of [Cr$_6$E$_8$(PEt$_3$)$_6$] (E = S, Se).

Introduction

Cluster molecules, composed of tens of atoms, have been considered as a linkage between molecular and solid-state chemistry.[1,2] Among these, an important subclass is metal chalcogenide bridged clusters, which have been reviewed under different subtopics in several publications.[3–6] Prominent representatives of this latter class are M$_6$E$_8$L$_6$ Chevrel-type cluster molecules with M mainly being a group 6, 8 or 9 metal atom and L being a phosphine or amine ligand.

Many examples have been synthesized and investigated among them the chromium chalcogenide clusters [Cr$_6$E$_8$(PEt$_3$)$_6$] (E = S, Se, Te)[7,8] and [Cr$_6$E$_8$H(PEt$_3$)$_6$] (E = S, Se),[9] which are the focus of this work. Recently, the cluster compounds [Cr$_6$Te$_8$(PEt$_3$)$_6$][8] and [Co$_6$E$_8$(PEt$_3$)$_6$] (E = Se,[10] Te[11,12])

were used in studies of the electrical properties of these molecules in molecular junctions[13] or in the crystal lattice.[14–16]

Although structurally related to solid state Chevrel phases,[17] the electronic situation is different for these molecular cluster compounds. In the neutral clusters [M$_6$E$_8$L$_6$], formally two M^{2+} and four M^{3+} can be assigned if the chalcogen atoms are assumed to be E^{2-} and the phosphine/amine ligands L to be neutral. Nevertheless, structural data (equal M–E, M···M and M–P bond distances) suggest an equal electron distribution leading to a formally broken oxidation state of +2.66 for each metal atom. The valence electron count for the M$_6$E$_8$ cluster core of group 6, 8 and 9 metal complexes amounts to 8 × 2e$^-$ for eight μ$_3$-E bridges, leaving 20, 32 or 38e$^-$ for possible M–M bonding. In this respect, Fan *et al.* already pointed out in a computational work that the degree and strength of M–M bonding interactions in these cluster complexes are difficult to determine.[18]

Magnetic properties have been studied in detail for [M$_6$S$_8$(PEt$_3$)$_6$] (M = Co, Fe) cluster molecules. The phenomenological description of an antiferromagnetic super-exchange by a spin Hamiltonian is complicated due to the number of paramagnetic centers, non-integer oxidation states and the delocalization of the unpaired spin density. Instead, reasonable quantitative rationalization of the magnetic properties has been achieved by SCF-Xα-SW and extended Hückel type calculations for [Co$_6$S$_8$(PEt$_3$)$_6$] (S = 0),[19,20] [Co$_6$S$_8$(PEt$_3$)$_6$]$^+$ (S = $\frac{1}{2}$),[19,21,22] and a series of related iron sulfide clusters [Fe$_6$S$_6$(PEt$_3$)$_6$]$^{n+}$ (n = 0, 1, 2, 3) (S = 3/2 (3+), 3 (2+), 7/2 (1+) and 3 (0)).[23,24]

[a]*Institut für Nanotechnologie, Karlsruher Institut für Technologie (KIT), Campus Nord, Hermann-von-Helmholtz-Platz 1, 76344 Eggenstein-Leopoldshafen, Germany. E-mail: andreas.eichhoefer@kit.edu; Fax: +49-(0)721-608-26368; Tel: +49-(0)721-608-26371*
[b]*Institut für Anorganische Chemie, Universität Würzburg, 97074 Würzburg, Germany*
[c]*Fachbereich Chemie, Universität Marburg, 35032 Marburg, Germany*
[d]*Karlsruhe Nano Micro Facility (KNMFi), Hermann-von-Helmholtz-Platz 1, 76344 Eggenstein-Leopoldshafen, Germany*

†Electronic supplementary information (ESI) available: Equations, crystallographic data, molecular structures, XRD powder patterns, magnetic data, and comprehensive data of quantum chemical calculations. CCDC 2172332–2172336. For ESI and crystallographic data in CIF or other electronic format see DOI: https://doi.org/10.1039/d2dt01690g
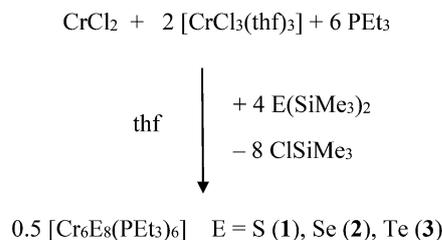
With respect to the chromium chalcogenide cluster molecules $[Cr_6E_8(PR_3)_6]$, Hessen *et al.* reported early on a paramagnetic behaviour for the tellurium bridged chromium cluster $[Cr_6Te_8(PEt_3)_6]$ with an effective magnetic moment of $\mu_{eff} = 2.8\mu_B$ from 100 to 300 K (corresponding to two parallel electronic spins if the paramagnetism is due to spin only).[8] Saito and co-workers also found a paramagnetic behaviour of the related sulfur and selenium bridged chromium clusters with a non-vanishing magnetic moment at 2 K which they interpreted as an indication of an $S = \frac{1}{2}$ ground state. They rationalized this observation by the postulation of an incorporated hydrogen atom in the cluster cages of $[Cr_6E_8(H)(PEt_3)_6]$ (E = S, Se)[9] supported by FAB mass spectrometry and CV measurements. In addition, they were able to synthesize and magnetically characterize the 'hydrogen-free' cluster $[Cr_6Se_8(PEt_3)_6]$ crystallizing in the space group $P\bar{1}$ which comprises nearest Cr···Cr distances that are longer by 14 pm compared to the trigonal ($R\bar{3}$) form of $[Cr_6Se_8(H)(PEt_3)_6]$. In agreement, they found an almost vanishing magnetic moment for the 'hydrogen-free' cluster at low temperatures.

Herein, we focus on a revised discussion with respect to the physical properties of the chromium chalcogenide cluster molecules $[Cr_6E_8(PEt_3)_6]$ (E = S, Se, Te) based on new temperature dependent structural data, quantum chemical calculations and comprehensive optical and magnetic measurements completed by a comparison with previous results from the literature.

Synthesis, structures and measurements

We developed a modified strategy for the synthesis of the chromium chalcogenide cluster molecules $[Cr_6E_8(PEt_3)_6]$ (E = S (**1**), Se (**2**), Te (**3**)), which results – especially for **2** – in improved yields (>40%) in comparison with previous reports (<21%). Main features are the use of mixtures of Cr(II) and Cr(III) metal salts in combination with silylated main group reactants $E(SiMe_3)_2$. The reactivity of the silyl chalcogenides $E(SiMe_3)_2$ (E = S, Se, Te) against the chromium metal salts increases distinctly from the sulfur to the tellurium compound, which is most probably related to the increased stability (covalent character) of the Si–S bond in comparison with the more ionic Si–Te bonding interaction. Silyl chalcogenides have been first used in the synthesis of chalcogenido materials by Steigerwald and coworkers[25] and subsequently established in the synthesis of metal chalcogenide cluster molecules by Fenske *et al.*[5,26–28]

$$CrCl_2 + 2\,[CrCl_3(thf)_3] + 6\,PEt_3$$

thf | + 4 E(SiMe_3)_2 / − 8 ClSiMe_3

$$0.5\,[Cr_6E_8(PEt_3)_6] \quad E = S\,(\mathbf{1}),\, Se\,(\mathbf{2}),\, Te\,(\mathbf{3})$$

From the reaction solutions (thf) the sulphide and selenide clusters **1a** and **2a** crystallize in the trigonal space group $R\bar{3}$

incorporating lattice solvent molecules whereas the telluride cluster **3** forms monoclinic crystals ($I2/a$) with no lattice solvent (Table S1†). We note that the lattice constants and packing of **3** measured at 180 K differ from the published structure in $I2/a$ measured at room temperature.[8] In single crystal and powder XRD measurements we found that there is a structural phase transition between these two forms upon cooling from 280 to 260 K accompanied by an ordering of a disordered phosphine ligand. The transition is only partially reversible and is accompanied by degradation of the long-range crystalline ordering.

Upon recrystallization of **1a** and **2a** in mixtures of thf/Et₂O/EtOH, triclinic crystals **1b** and **2b** of the respective isostructural cluster molecules were obtained, and contain no solvent molecules in the crystal lattice.

The main structural characteristics of the cluster structures have been discussed in detail in several preceding papers (Fig. 1).[7–9] Formally, six chromium atoms, which are arranged at the corners of an octahedron, are μ_3 bridged by eight chalcogen atoms over the trigonal faces which themselves form a cube. Including the terminal phosphine ligands, each chromium atom possesses an unusual square pyramidal coordination environment formed by four chalcogen atoms and one phosphorous atom. As noted above, if one assigns formally two negative charges to the chalcogen atoms (μ_3-E^{2-}) the chromium atoms must be formally mixed valence ($2 \times Cr^{2+}$ and $4 \times Cr^{3+}$). However, the structural characteristics (and also the quantum chemical calculations) suggest an equal delocalisation of 20 valence electrons over the six chromium atoms.

The structural parameters of the trigonal forms **1a** and **2a** and the triclinic form **2b** as found by us are similar to those published earlier by Saito and co-workers (Table 1 and Table S2†).[7] For complex **1b**, no corresponding triclinic form has been reported until now. Interestingly, in a successive paper[9] the triclinic form (herein named **2b**) was published by Saito and co-workers with similar lattice constants but with Cr···Cr distances elongated by more than 14 pm in compari-
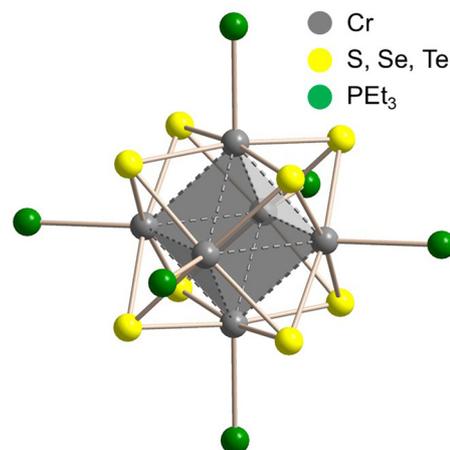

Fig. 1 Schematic molecular structures of **1a**, **2a**, **1b**, **2b** and **3**.

Table 1 Comparison of the structural parameters[a] in **1–3** with those from the literature

	Space group	Reference	T [K]	Cr–E	Cr⋯Cr	E⋯E	Cr–P
1a	$R\bar{3}$	This work	180	233.03–234.94(6)	259.38–260.45(5)	329.0–330.9	239.33(5)
1b	$P\bar{1}$	This work	180	232.79–234.56(4)	256.77–259.51(3)	328.6–331.1	241.20–242.13(4)
$[Cr_6S_8(PEt_3)_6]$	$R\bar{3}$	7	[b]	232.7–234.2(2)	259.2–259.6(1)	328.7–329.9	239.5(1)
2a	$R\bar{3}$	This work	180	243.18–245.22(5)	264.98–265.45(6)	344.6–345.1	240.92(6)
2b	$P\bar{1}$	This work	180	244.25–245.79(8)	265.95–267.98(9)	343.8–346.7	241.25–241.68(12)
$[Cr_6Se_8(PEt_3)_6]$	$R\bar{3}$	7	[b]	244.1–246.8(2)	267.2–268.3(3)	345.4–346.2	242.8(3)
$[Cr_6Se_8(H)(PEt_3)_6]$	$R\bar{3}$	9	293	244.1–246.1(1)	265.5–265.6(1)	346.0–346.1	240.3(2)
$[Cr_6Se_8(PEt_3)_6]$	$P\bar{1}$	7	[b]	245.1–246.5(2)	269.8–271.2(3)	344.7–347.9	241.3–242.4(4)
$[Cr_6Se_8(PEt_3)_6]$	$P\bar{1}$	9	226	245.8–247.7(2)	279.6–282.6(1)	345.0–348.4	240.5–241.1(2)
3 (cell 2)	$C2/c$	This work	150	264.55–266.60(7)	281.58–285.70(8)	372.1–378.5	243.93–244.66(11)
3 (cell 1)	$I2/a$	8	293	263.9–266.2(4)	289.6–295.3(5)	371.3–379.6	242.8–243.6(6)

[a] T: measurement temperature; atomic distances [pm]. [b] Not given.

son with our results and the structure published before.[7] Based on the magnetic measurements and FAB mass spectrometry, the authors revised their former discussion with respect to the composition of the $[Cr_6E_8(PR_3)_6]$ (E = S, Se; R = organic group) cluster molecules. For the trigonal forms of these cluster molecules they now propose the incorporation of a hydrogen atom in the center of the cluster which could be removed in the case of the chromium selenide cluster in an oxidation reaction with $[FeCp_2](PF_6)$ yielding triclinic $[Cr_6Se_8(PEt_3)_6]$ (herein named **2b**) with elongated Cr⋯Cr distances. For our reactions the inclusion of a hydrogen atom in the chromium chalcogenide cluster molecules $[Cr_6E_8(PEt_3)_6]$ (E = S, Se) is somewhat unlikely as it has not been observed in reactions similar to our procedure with other metal salts before by us and others.[5,26–28] Furthermore, it is contradictory that a similar reaction of the hydrogen containing sulfide bridged cluster $[Cr_6S_8(H)(PEt_3)_6]$ with $[FeCp_2](BF_4)$ was later on reported to yield the ionic cluster $[Cr_6S_8(H)(PEt_3)_6]^+(BF_4)^-$.[29] In this case, instead of the removal of the central hydrogen, a one electron oxidation of the neutral starting cluster takes place which also results in an elongation of the Cr⋯Cr distances.

In a theoretical work, Ahlrichs and coworkers pointed out that the Cr⋯Cr distances calculated for $[Cr_6S_8(PEt_3)_6]$ by DFT (BP86/SV(P)) are found to be shorter by up to 14 pm than the experimentally observed ones whereas for the Cr–P and Cr–S bond distances they agree within 5 pm.[18] The deviation of the Cr⋯Cr distances is atypical of the method and in addition it has not been found for the structurally related cobalt and molybdenum cluster complexes (M⋯M distances in $[Mo_6S_8(CO)_6]$ are overestimated by 3 pm which is usual for the employed method).

These unclarified results of the quantum chemical calculations and our estimation that the inclusion of a hydrogen atom in the chromium chalcogenide cluster molecules $[Cr_6E_8(PEt_3)_6]$ (E = S, Se) is somewhat unlikely stimulated us to revise the original experimental and theoretical investigations. In the course of these investigations we found as a major observation that, when measuring temperature dependent single crystal data for the 'solvent-free' crystals of **1b** and **2b**, the Cr⋯Cr distances on trend experience a much larger

increase (~4.5 pm) upon warming (120 K, 200 K and 280 K) than the Cr–E, Cr–P and E⋯E distances (<0.68 pm) do (Fig. 2 and Table S3†). This finding will be discussed further in more detail in view of the results from the quantum chemical calculations in the respective section.

The measured powder X-ray diffraction (XRD) patterns of **1a**, **1b**, **2a** and **2b** synthesized by us show a good agreement with the calculated ones based on the single crystal data (Fig. S1–S4†). The room temperature XRD powder pattern of **3** corresponds to the calculated one of the monoclinic phase published in the literature.[8] Upon cooling, the pattern starts to
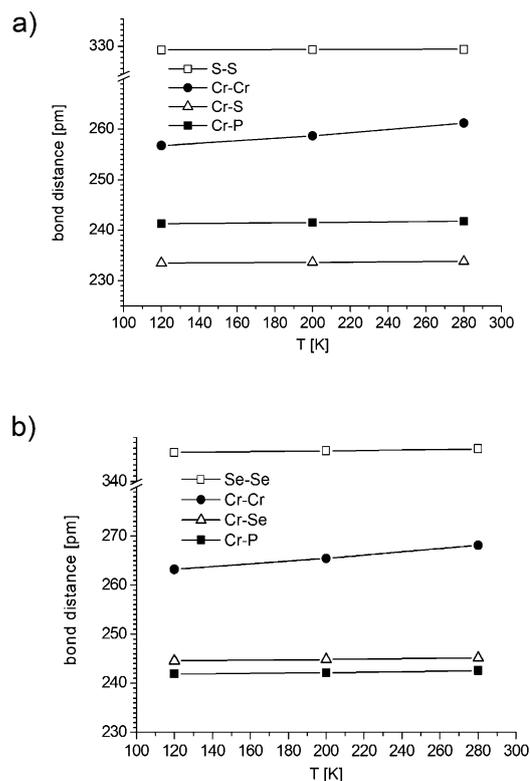

Fig. 2 Mean atomic distances [pm] in (a) **1b** and (b) **2b** measured at 120, 200 and 280 K (see also Table S3, ESI†).

gradually change and resembles at 250 °C the one calculated for the structure of **3** measured at 150 K (Fig. S4†). Slightly increasing differences in the position of the peaks of **1a**, **1b**, **2a** and **2b** with increasing detection angle arise from the temperature difference between data collections (single crystal XRD at 180 K *vs.* powder XRD at room temperature).

C, H, and S elemental analyses (see the Experimental section) and TGA measurements (Fig. S5†) of **1a** and **2a** suggest that thf (~1.5 eq.) remains even after vacuum drying of the microcrystalline powders.

ESI-TOF mass spectra

ESI-TOF mass spectra were recorded for toluene solutions of **1a**, **1b**, **2a**, **2b** and **3**. Molecular ion peaks of the clusters were detected in positive ion mode comprising broad isotopic patterns (Fig. 3 and S6, S7†). The spectra of the compositional analogues **1a**/**1b** or **2a**/**2b** are found to be identical. A moderate tendency for fragmentation confirms the stability of the molecules in solution already pointed out by Steigerwald and coworkers.[8]

The mass spectra of complex **1** display a molecular ion peak which slightly varies upon prolonged measurement time in the intensity distribution and position (Fig. 3 and S6†). Probably the samples contain traces of Cl⁻ ions which lead upon an exchange against sulphur ions in solution or the gas phase to the additional formation of $[Cr_6S_7Cl(PEt_3)_6]^+$ (m/z 1280.96) cluster cations. In comparison with the neutral starting cluster **1a** these species are intrinsically charged and will thus lead to an increased signal intensity compared to the cluster cation $[Cr_6S_8(PEt_3)_6]H^+$ (m/z 1277.98) although their absolute concentration is much lower.

For solutions of **2** we observed that the intensity distribution of the molecular ion peak corresponds to the charged fragment $[Cr_6Se_8(PEt_3)_6]H^+/[Cr_6Se_8(H)(PEt_3)_6]^+$ (m/z 1653.65).

In addition, a slight tendency of fragmentation of the cluster is detected (Fig. 3 and S7;† Table 2). The corresponding peaks of much lower intensity can be simulated by cluster fragments, which contain oxygen and chlorine atoms most probably resulting from an oxidation of the phosphine ligand and/or an exchange of Cl⁻ against S²⁻ ions.

The telluride cluster **3** displays a molecular ion peak which corresponds well in terms of its position and intensity distribution to the simulation of the singly charged cluster $[Cr_6Te_8(PEt_3)_6]^+$ (m/z = 2043.43). This observation suggests a relatively low oxidation potential of the cluster in line with the reported facile synthesis of the charge transfer salt $[Cr_6Te_8(PEt_3)_6]·2C_{60}$ upon reaction of the cluster with two equivalents of the fullerene in solution.[14]

Therefore, with respect to the mass spectra, the incorporation of an H atom, which was proposed by Saito and coworkers for **1a** and **2a**, is at least improbable for **3**. For **1a** and **2a** the results from mass spectrometry do not allow for a clear differentiation between the situations that the molecular ion peak results from an ionization of the cluster which already
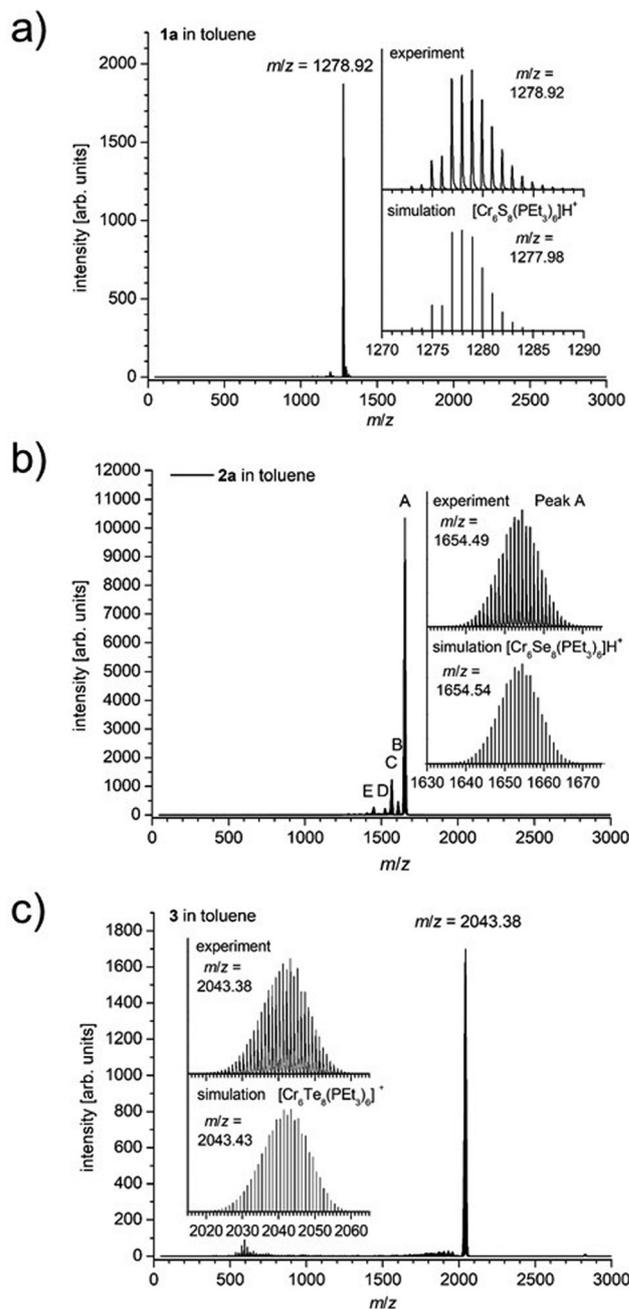

Fig. 3 ESI-ToF mass spectra of (a) **1a**, (b) **2a**, and (c) **3** in positive ion mode (see also table 2).

incorporates a hydrogen atom $[Cr_6E_8(H)(PEt_3)_6]^+$ (E = S, Se) or results from the common case that neutral molecules are 'ionized' by the uptake of a proton forming $[Cr_6E_8(PEt_3)_6]H^+$ (E = S, Se).

UV-Vis-NIR spectroscopy

The UV-Vis-NIR spectra of **1a**, **2a** and **3** were recorded for solutions in toluene in transmission mode and in reflection mode for the solid state both as a mull in nujol and for microcrystal-

Table 2 Assignment of ion peaks in the ESI-ToF mass spectra of **2a** [a]

Experiment		Simulation	
Peak	m/z		m/z
A	1654.49	$[Cr_6Se_8(PEt_3)_6]H^+$	1654.54
B	1608.55	$[Cr_6Se_7Cl(PEt_3)_6]^+$	1608.58
C	1568.41	$[Cr_6Se_8(PEt_3)_6(OPEt_3)_2]H^+$	1568.44
D	1522.47	$[Cr_6Se_7Cl(PEt_3)_3(OPEt_3)_2]^+$	1522.48
E	1450.36	$[Cr_6Se_8(PEt_3)_2(OPEt_3)_2]H^+$	1450.35

[a] Toluene solution.

line powders in a cuvette (Fig. 4 and S8, S9†). The solution spectra display a more or less featureless increase of the absorbance on going from 0.5 eV up to 4.5 eV, which is in agreement with the results from the literature.[7,8] The spectra recorded for concentrated solutions support the observation of measurable absorbance (>100 l mol^{-1}cm^{-1}) down to 0.5 eV. These findings are further corroborated by the measurements on solid samples especially by the reflection measurements performed on the microcrystalline powders in quartz cuvettes (Fig. 3). When compared to the spectrum of CdSe recorded in the same sample environment, **1a**, **2a** and **3** clearly display intensity down to 0.5 eV whereas for CdSe one measures the expected band gap at around 1.6 eV. Therefore, the optical spectroscopic investigations reveal the existence of energetically low-lying excited states in these cluster complexes.

Magnetic measurements

Dc magnetic data of **1a**, **1b**, **2a**, **2b** and **3** were measured between 2 and 300 K in a field of 0.1 T and magnetization measurements were carried out from 0 to 7 T at 2, 3, 4, 6, 10 and 25 K.
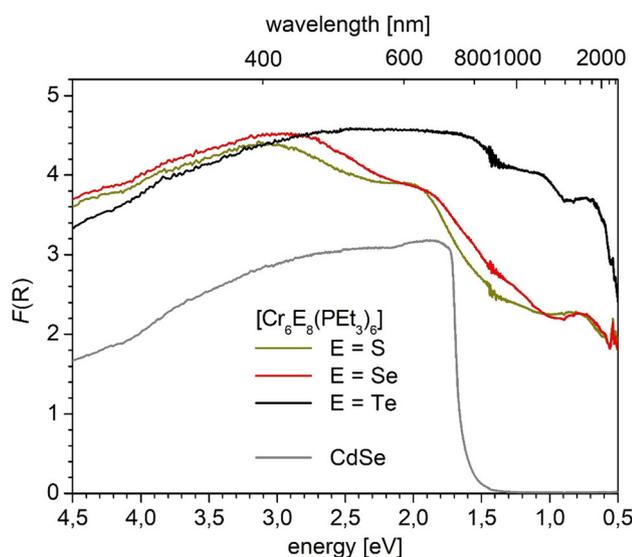

Fig. 4 Reflection UV-Vis NIR spectra of **1a**, **2a** and **3** in the solid state as microcrystalline powders in quartz cuvettes compared to the spectrum of CdSe.

The graphs of χT vs. T for **1a**, **1b**, **2a**, **2b** and **3** display a gradual decrease from room temperature down to 2 K (Fig. 5). Among these, **3** displays the largest spread from 1.684 cm^3 mol^{-1} K at room temperature down to 0.230 cm^3 mol^{-1} K at 2 K. The curves of **1a**, **1b**, **2a** and **2b** display comparably lower room temperature values but higher low temperature ones.
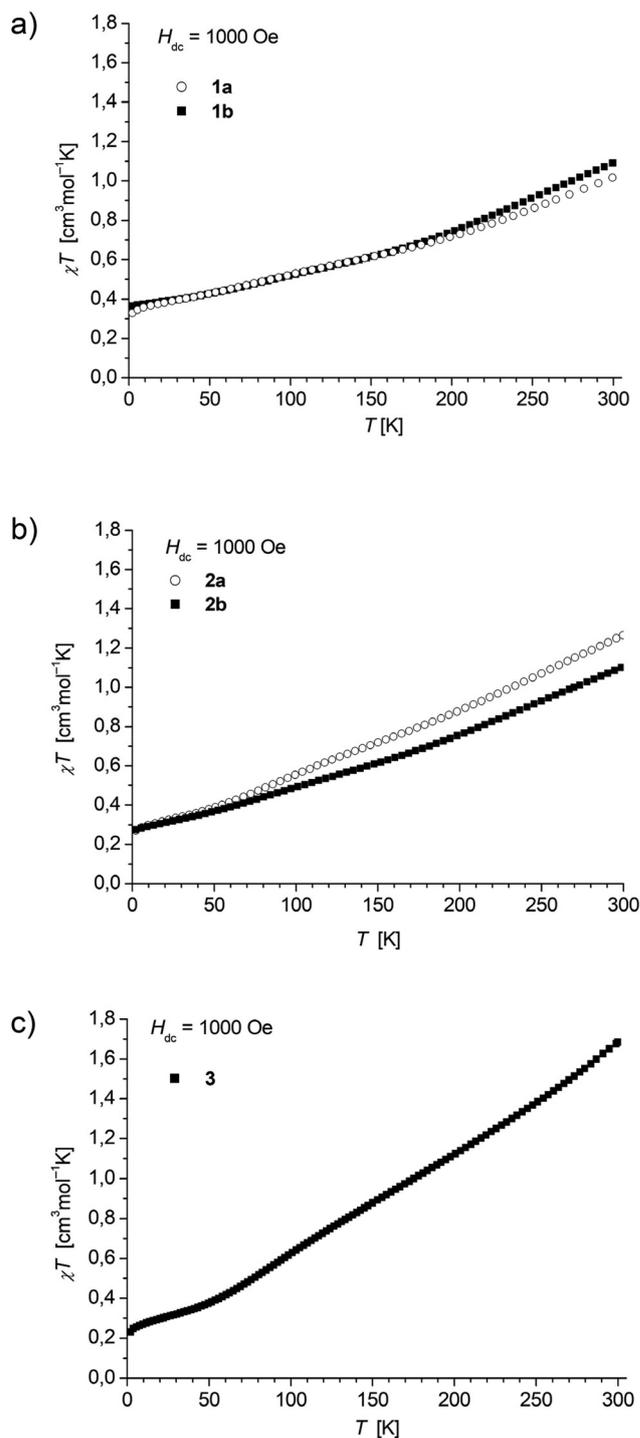

Fig. 5 Temperature dependence of χT of (a) **1a** and **1b**, (b) **2a** and **2b**, and (c) **3**.

The low temperature behaviour therefore suggests for all complexes a non-vanishing moment originating from a ground state $S \neq 0$ with values of χT at 2 K for **1a** (0.366), **1b** (0.347), **2a** (0.288) and **2b** (0.276) which are close to the theoretical spin-only value calculated for $S = 1/2$ (0.375 cm^3 mol^{-1} K). In complexes with more than one magnetic ion, such a decrease of χT can be assigned to antiferromagnetic coupling but in our case no linear Curie Weiss behaviour of χ^{-1} is observed (Fig. S10†).

The magnetization curves of **1a**, **1b**, **2a**, **2b** and **3** at 2 K show no clear saturation behaviour and all reveal values of the saturation magnetization M_S at 7 T well below the theoretical value of $1N_A\mu_B$ for a $S = \frac{1}{2}$ ground state (Fig. S11†). There seems to be a trend that the sulfide-bridged clusters **1a** and **1b** saturate at higher M_S values (0.78 and 0.86$N_A\mu_B$) than the two selenide ones **2a** and **2b** (0.67 and 0.64$N_A\mu_B$) followed by **3** with a value of 0.37$N_A\mu_B$ at 7 T and 2 K.

Reduced magnetization data resulting from variable field dependent measurements of **1a**, **2a** and **3** at different temperatures all show a superposition of the curves (Fig. S12†). This is indicative of the absence of magnetic anisotropy. Furthermore, field dependent ac measurements have been performed for **1a**, **2a** and **3** in a range from 0 to 5000 Oe at 2 K using a 3.0 Oe ac field, oscillating in an extended range of frequencies between 1 and 1500 s^{-1}. The out-of-phase component of the ac susceptibility (χ'') of all complexes has much lower intensity than the in-phase component (χ') and displays no maximum indicating that the spin lattice relaxation is faster than the timescale of the experiment.

The measured curves of χT *vs. T* roughly agree for **1a** and **2a** with the ones published in the literature[9] (for better comparison *T*-dependent μ_{eff} values are plotted in Fig. S13;† magnetization measurements (M_S *vs. H*) have not been reported so far). In contrast, for **3** a more or less constant magnetic moment of approximately 2.8μ_B down to 100 K was reported[8] whereas we observe a constant decrease of the moment from 3.67μ_B at rt down to 1.36μ_B at 2 K.

A comprehensive magnetic modelling of the hexanuclear cluster complexes would include six magnetic centres each comprising a theoretical spin of $S = 3.333$ interacting through 24 couplings of equal strength *via* the eight μ$_3$-Se bridges. Any possible direct interactions between the chromium atoms would further complicate this model. A complete antiferromagnetic super-exchange of all unpaired spins (an even number of similar paramagnetic centers with similar spin numbers through an even number of bridges) could result in a spin ground state of $S = 0$. The molecular orbital (MO) diagram derived for [Cr$_6$S$_8$(CO)$_6$] predicts such a $S = 0$ ground state with the HOMO (21 t$_{1u}$) filled by six electrons and the LUMO (13 e$_g$) being ~0.65 eV or above.[18] Such an experimental behaviour is reported for [Mo$_6$E$_8$(PEt$_3$)$_6$] (E = S, Se).[30,31]

In view of the non-vanishing moments for the sulfide and selenide bridged chromium clusters **1a** and **2a**, Saito and co-workers therefore postulated the existence of an additional hydrogen atom for the cluster structures crystallizing in the trigonal space group $R\bar{3}$ [Cr$_6$E$_6$(H)(PEt$_3$)$_6$] (E = S, Se).[9] This suggestion was additionally supported by FAB mass spectroscopy

and CV measurements. A total of 21 cluster core electrons would rationalize the non-vanishing moment at low temperatures. In agreement with this assumption, the 'hydrogen-free' cluster with extended Cr⋯Cr distances which crystallizes in the triclinic space group $P\bar{1}$ was found by them to approximately display the expected behaviour of an $S = 0$ ground state.

We observed for both pairs of the two different crystallographic forms **1a**/**1b** and **2a**/**2b** a similar magnetic behaviour with non-vanishing magnetic moments at low temperatures in line with the fact that the Cr⋯Cr distances are in our case quite similar in between such pairs.

Following the findings of Saito and co-workers this would mean that in our case also the triclinic forms **1b** and **2b** should incorporate hydrogen atoms because the 'hydrogen-free' variant of the cluster which crystallizes with almost the same lattice parameters as **2b** (Tables S1 and S2†) should comprise extended Cr⋯Cr distances and a vanishing magnetic moment at low temperatures.

Electron paramagnetic resonance (EPR) spectroscopy

Characterization of complexes **1a**, **2a** and **3** by EPR spectroscopy as microcrystalline powders reveals a strongly temperature-dependent behaviour (Fig. S14–S16†). An EPR signal is only observed below 40 K, and gradually increases as the temperature is lowered from 40 K to 10 K. The temperature dependent spectra of **1a** in frozen toluene solution reveal a similar behaviour with more clearly resolved peaks (Fig. S17†). The disappearance of the EPR signal at higher temperatures is indicative of short electron relaxation times being typical of unpaired electrons at many transition metal sites including Cr^{2+} and supports herein the suggestion of their delocalization over the whole cluster molecule.[32] A similar temperature behaviour has also been reported for the EPR spectra of the isostructural but cationic cobalt cluster [Co$_6$S$_6$(PEt$_3$)$_6$]$^+$.[19,22]

The solid-state EPR spectra of **1a**, **2a** and **3** exhibit relatively broad signals, which are spread over a g value range of 1.9 to 2.6, indicating an anisotropic electron distribution in the complexes. Both the anisotropic features in conjunction with the temperature dependence are not in agreement with an $S = 1/2$ spin state and localization of an unpaired electron at a hydrogen atom encapsulated in the cluster.[32]

Indications of the existence of higher spin states ($S = 1$ or higher) are not readily apparent.[33] The solid state spectra of the selenium cluster **2a** display only very weak half-field transitions (see Fig. S15†), whereas for **1a** and **3** they are hardly detectable. Additionally, the main spectral features that are closely distributed around $g = 2$ suggest only a small zero-field splitting. Given that no other spectral features are observed in the field range of 0–1000 mT, we therefore conclude that a clear assignment of the EPR spectra with respect to the spin state of **1a**, **2a** and **3** at low temperature is not possible. The analysis of the temperature-dependent signal intensities could provide further insight but would necessitate an understanding of the exchange interactions between the chromium atoms in the cluster.

Quantum chemical calculations

Quantum chemical calculations (for details see the Experimental section) were performed in order to assist the interpretation of the experimental observation that the chromium chalcogenide cluster molecules **1a**, **1b**, **2a**, **2b** and **3** possess non-vanishing magnetic moments at low temperatures. First, we started with a plausibility consideration for the incorporation of a hydrogen atom as suggested by Saito and coworkers.[9]

The bond energies of a hydrogen atom in $[M_6E_8(PEt_3)_6]$ (M = Cr, Mo; E = S, Se) have been calculated as the energetic difference of the reaction $M_6E_8L_6 + H \rightarrow M_6E_8HL_6$ and are listed in Table S4.† They reveal that such an incorporation would be energetically favourable for the two chromium chalcogenide cluster molecules by more than 240 kJ mol^{-1} and even for a cleavage of H_2 by more than 40 kJ mol^{-1}. However, based on the results they would also be equally possible for the related molybdenum cluster complexes. Contradictorily, the molybdenum clusters have all been reported to be diamagnetic.[30,31]

As noted above, structural parameters have been calculated by Ahlrichs and coworkers for the $[Co_6E_8(PMe_3)_6]$ (E = S, Se, Te), $[M_6S_8(PMe_3)_6]$ (M = Cr, Mo, W, Rh) and $[Cr_6S_8(PEt_3)_6]$ cluster molecules, albeit with a single and rather cheap method (by today's standards).[18] The atomic distances were found to be in reasonable agreement with the experimental values with the exception of the Cr···Cr distances in $[Cr_6S_8(L)_6]$ (L = PMe_3, PEt_3) which are calculated to be up to 14 pm shorter than the experimentally observed ones being atypical of this method.

In order to examine this discrepancy further, the closed shell states (CS) of **1** and **2** were first calculated by the use of three different functionals, namely PBE, PBE0 and B3LYP

(Table S5†) and by employing more flexible def2-TZVP basis sets. The values for the mean Cr···Cr distances in **1** are comparable to those calculated by Ahlrichs (246.0–247.8 pm)[18] all being shorter than the experimental value at 120 K (256.74 pm) and the shortest for PBE0 (244.82 pm). All other mean atomic distances (Cr–P, Cr–E and E···E) calculated for the closed shell state by PBE/def2-TZVP display a good agreement with the experimental values (Table 3).

The consideration of an incorporated hydrogen atom in the center of **1** and **2** (denoted CS···H) results in an extension of the calculated Cr···Cr distances by ~5 pm, approaching the experimental findings (Table 3). This behaviour can be rationalized by the calculated molecular orbital (MO) diagrams of **1** and **2** (Fig. 6). They reveal a similar situation to that calculated for $[Cr_6S_8(CO)_6]$ before.[18] The HOMO is formed by three energetically degenerate orbitals of a_u symmetry (**1**: 166, 167, 168; **2**: 202, 203, 204). These are mainly localized at the chromium atoms and to a lower extent also on the chalcogen atoms (Fig. 7 and S18, Table S6†). The LUMO is formed by two energetically degenerate orbitals of a_g symmetry (**1**: 167, 168; **2**: 203, 204) which are Cr···Cr antibonding. Therefore, an additional electron is expected to occupy a slightly antibonding a_g orbital. However, this contrasts Saito's work, who postulated on the basis of the experimental findings the inverse behaviour that is a distinct reduction of the Cr···Cr distances by up to 15 pm upon insertion of the hydrogen in the center (for details also see the discussion in the section Syntheses and structures).[9]

The calculated small HOMO–LUMO gaps (PBE, **1**: 0.655 eV, **2**: 0.688 eV) are roughly in line with the appearance of the experimental optical reflection spectra (Fig. 4). For a more precise comparison, dipole-active singlet transitions have been calculated with TDDFT (PBE) for **1** and **2** and compared with the experimental spectra of **1a** and **2a** (Fig. 8 and 9, Table S7†).

Table 3 Calculated energy differences ΔE^a [kJ mol^{-1}] between the excited states^b and the $S = 0$ state and mean values of the calculated atom distances [pm] in **1** and **2** compared to the experimental values at 120 K^c

| | Theory | | | | Experiment |
	$S = 0$	$S = 1/2$ (CS · H)^d	$S = 1$	$S = 2$	120 K
	1				
ΔE			30.5	38.8	
Cr–P	242.31 ± 0.09	240.00 ± 0.61	241.64 ± 1.68	241.94 ± 0.13	241.26 ± 0.43
Cr–S	231.44 ± 0.29	232.55 ± 0.92	231.36 ± 1.22	232.40 ± 0.55	233.50 ± 0.54
Cr···Cr	248.57 ± 0.12	253.50 ± 1.53	252.49 ± 1.96	254.77 ± 2.56	256.74 ± 0.73
E···E	326.83 ± 0.06	328.16 ± 2.56	326.44 ± 3.36	327.82 ± 0.52	329.34 ± 0.95
	2				
ΔE			25.9	−2.43	
Cr–P	243.55 ± 0.08	241.00 ± 0.64	243.38 ± 0.45	243.66 ± 1.16	241.89 ± 0.38
Cr–Se	243.80 ± 0.38	244.78 ± 0.88	244.41 ± 1.30	246.79 ± 0.45	244.56 ± 0.54
Cr···Cr	254.14 ± 0.10	259.32 ± 1.44	256.62 ± 3.50	268.91 ± 4.09	263.55 ± 0.68
E···E	344.63 ± 0.16	345.85 ± 2.28	345.40 ± 4.70	348.19 ± 1.31	345.24 ± 0.73

^{a} $\Delta E = E_{exc} - E_{cs}$ (cs = closed shell; exc = excited state). ^{b} $S = 1$ and $S = 2$ denote the excited triplet and quintet states, respectively. ^{c} Calculated (PBE/TZVP) for different energy states. ^{d} $S = 0 \cdot H$: denotes the closed shell state with a hydrogen atom in the centre of the cluster.
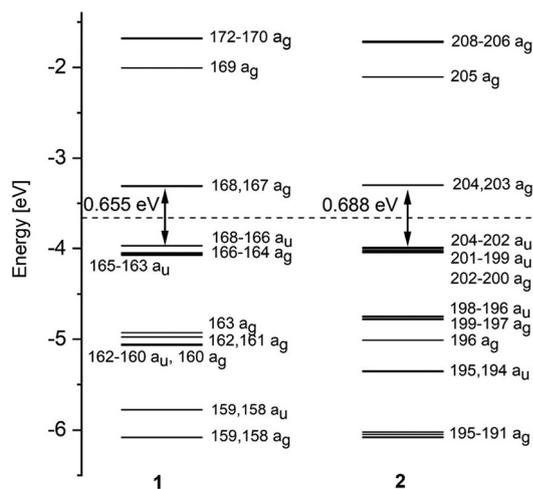
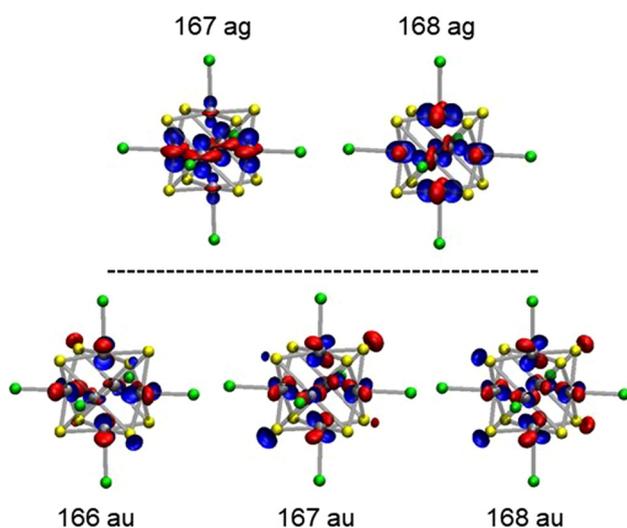**Fig. 6** MO diagrams of **1** and **2** (PBE/def2-TZVP).

Fig. 7 Molecular frontier orbitals of **1** (occupied in the lower row; unoccupied in the upper row). Contours are drawn at 0.06 (red) and −0.06 (blue) atomic units [a.u.].

Fig. 8 Experimental and calculated (TDDFT/PBE) electronic spectra of **1a**. Panels from top to bottom: experimental spectra in diluted and concentrated solutions of toluene. Calculated singlet excitation energies (green lines) and corresponding simulated spectra (black lines) with superimposed Gaussians of FWHM = 0.5 eV (linear scale) and 0.3 eV (log scale). UV-Vis-NIR reflection spectra at 295 K (microcrystals in a quartz cuvette). The character of transitions up to 1.4 eV is visualized using the difference of electron densities for the excited band and the ground state. The contributions of occupied orbitals are plotted in red and those of the unoccupied orbitals in blue.

Similar results are obtained with PBE0 and B3LYP (Fig. S19†). By plotting the calculated and simulated patterns on a logarithmic scale we achieved a better comparability in terms of the intensities with the experimental reflection spectra. Reasonably in line with the experimental patterns, the lowest energy transitions have been calculated at 0.68 and 0.71 eV (PBE) for **1** and **2,** respectively (Table S7†). Differences in the energetic position of the band maxima of the experimental and theoretical spectra (as far as identifiable) might be rationalized by the difference in temperature between the calculated (0 K) and the experimental patterns (rt) which could lead to different electronic situations as indicated by temperature dependent magnetic measurements.

The character of the lowest energy transitions is mostly of metal to metal type (for frontier orbitals see Fig. 7 and S18,
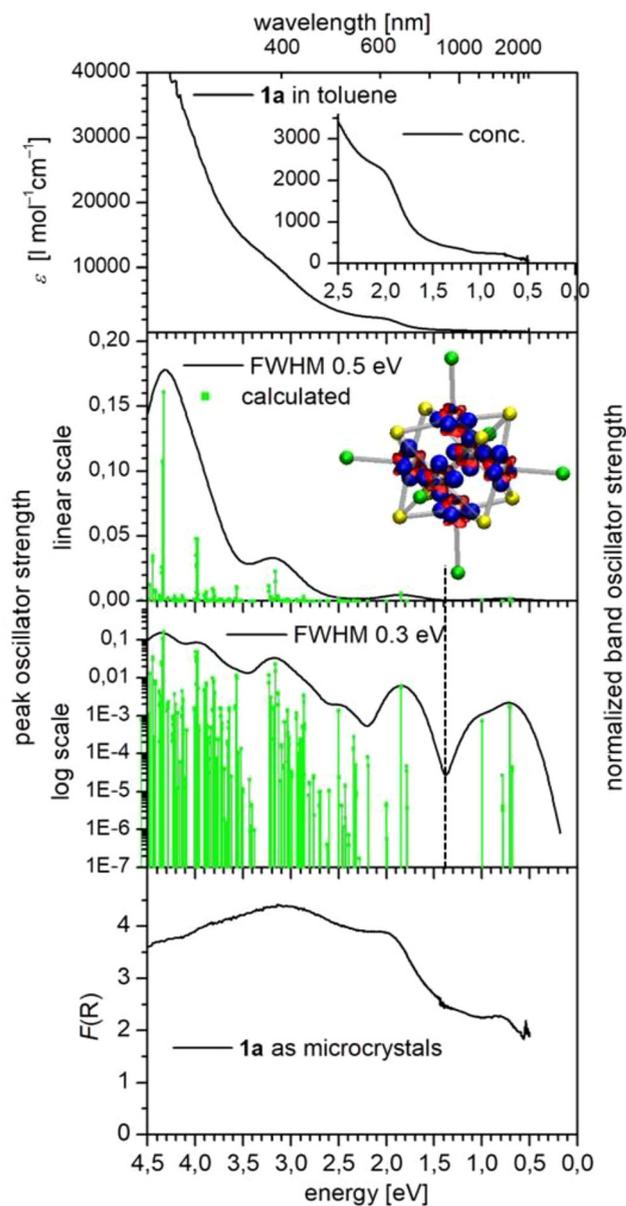
Table S6, S7†). All clusters belong in principle to Robin–Day class III of mixed-valence compounds (delocalized electrons in clusters with equivalent and indistinguishable ions), which display distinct intervalence bands ($\varepsilon_{max} \gg 5000$ l mol^{-1}cm^{-1}).[34,35] Extinction coefficients for the optical transitions in the low energy region (<1 eV) are found for **1–3** in
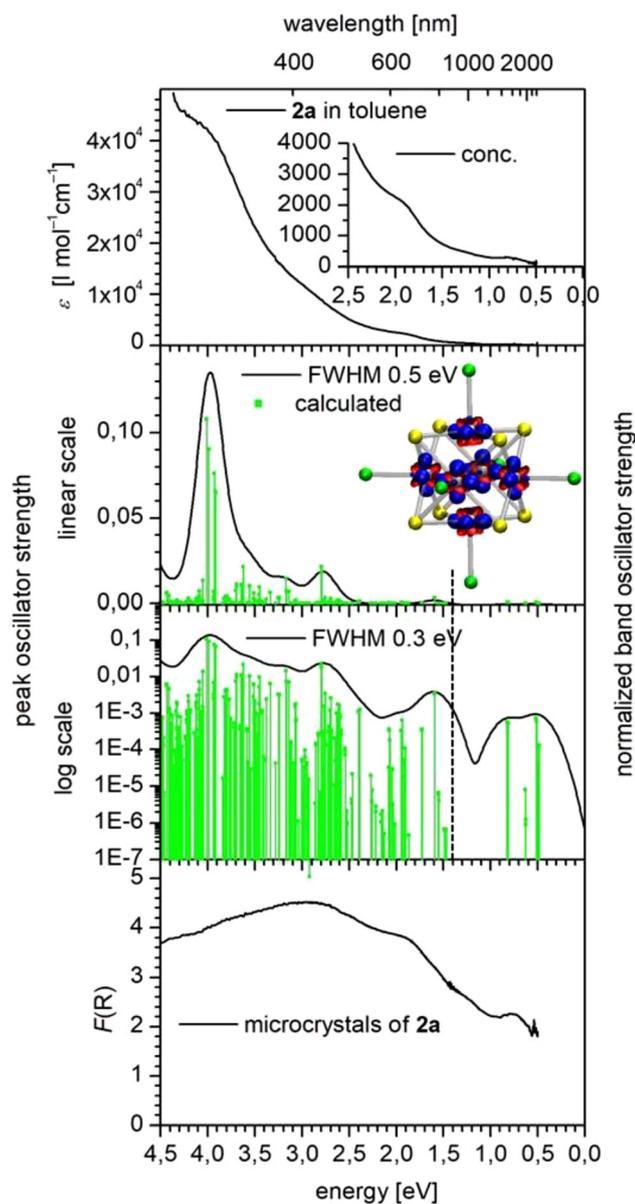
Fig. 9 Experimental and theoretical (TDDFT/PBE) electronic spectra of **2a**. Panels from top to bottom: experimental spectra in diluted and concentrated solutions of toluene. Calculated singlet excitation energies (green lines) and corresponding simulated spectra (black lines) with superimposed Gaussians of FWHM = 0.5 eV (linear scale) and 0.3 eV (log scale). UV-Vis-NIR reflection spectra at 295 K (microcrystals in a quartz cuvette). The character of transitions up to 1.4 eV is visualized using the difference of electron densities for the excited band and the ground state. The contributions of occupied orbitals are plotted in red, and those of the unoccupied orbitals in blue.

the range of $200 < \varepsilon < 600$ l $mol^{-1}cm^{-1}$ which is the border region between very strong but Laporte forbidden d–d transitions and weak but allowed charge-transfer bands (Fig. S8(a)†). In agreement, the calculations also predict very low intensities for the lowest energy transitions $f < 1 \times 10^{-3}$ (Table S7†).

The above findings of (a) small HOMO–LUMO gaps, (b) sensitivity of the Cr⋯Cr atom distance to the addition of an extra electron and (c) distinct T-dependence of the Cr⋯Cr atom distance suggest the possible relevance of energetically low-lying excited states in **1–3**. Therefore, structural parameters were calculated for the excited state structures of **1** and **2** with triplet (S = 1) and quintet (S = 2) occupation by three different functionals (PBE, PBE0, B3LYP) and compared to the closed shell state (CS) (Table 3, S5 and S8†). The results of the calculations obviously critically depend on the functional used, in particular on the amount of admixed Hartree–Fock exchange (Tables S5 and S8†). PBE0 and B3LYP yield Cr⋯Cr atom distances that overestimate the measured distances by 25–40 pm for the S = 1 and the S = 2 states of **1** and **2**, see Table S5,† whereas deviations with the PBE functional amount to only 6 pm at most. Furthermore, B3LYP and PBE0 predict the S = 1 and S = 2 states to be much more stable than the S = 0 state, see Table S8,† which – together with the errors for the Cr⋯Cr distances for these states – demonstrates these functionals to be much less suited for the present case. In the following, only the PBE results will be discussed.

In contrast to the clear effect on the Cr⋯Cr atom distances (elongation by up to ∼6 and 14 pm in the quintet state of **1** and **2** compared to the singlet state), other atom distances (Cr–P, Cr–S, E⋯E) display much smaller maximum changes (**1**: ±1 pm, **2**: ±3.5 pm) upon excitation (Table 3). This fits to the occupation of antibonding (**1**: 167, 168 a_g; **2**: 203, 204 a_g) orbitals which are mainly localized at the chromium atoms upon going from the closed shell to the excited state structures (Fig. 6, 7 and S18, Table S6†). Moreover, these findings now help to rationalize the temperature dependent structural data, which reveal a stronger increase of the Cr⋯Cr atom distance upon going from 120 to 280 K than those of the Cr–P, Cr–S and E⋯E distances (Table S3†). The population of the antibonding orbitals increases with increasing temperature. The situation is therefore roughly comparable with a low spin (S = 0) / high spin (S = 2) transition in a complex of a d^6 transition metal ion. Only roughly because the dc magnetic measurements of **1** and **2** reveal that this transition is very broad and not completed at both ends of the temperature range from 2 to 300 K (2 K $S \sim \frac{1}{2}$, 300 K $S \geq 1.2$). Therefore, the electronic configuration of **1** and **2** in this temperature range might be better described as a sort of a temperature dependent intermediate spin state $S \sim 1$ being in fact most probably a mixture of states (S = 0, 1, 2).

In contrast, exploratory calculations for the molybdenum cluster $[Mo_6S_8(PEt_3)_6]$ reveal that only the diamagnetic state fulfills the *Aufbau* principle, as the exchange energy between the electrons of the same type is lower for 4d than for 3d elements. This is in line with a slightly larger (0.833 eV) HOMO–LUMO gap for $[Mo_6S_8(PEt_3)_6]$ than for the chromium analogue **1** and clearly supports the experimental findings of a diamagnetic behaviour.[30,31]

Dipole allowed spin-conserving transitions were calculated for the quintet state of **2**. These reveal slight differences in comparison with the spectra of the closed shell state especially visible in the low energy region (Fig. S20†). However, because

the experimental bands are extremely broad and featureless and more importantly cannot be detected further down than 0.5 eV due to limitations of the instrumental setup and the occurrence of vibrational overtones, a comparison with these calculated excited state spectra does not allow for further conclusions.

Conclusion

The inclusion of a hydrogen atom in the chromium chalcogenide cluster molecules $[Cr_6E_8(PEt_3)_6]$ (E = S, Se), which was proposed previously, is rather unlikely for several reasons. First of all, it has not been observed in reactions similar to our procedure with other metal salts reported before by us and others.[5,26,27] Next, it is unlikely that the oxidation of $[Cr_6Se_8(H)(PEt_3)_6]$ with $[FeCp_2]PF_6$ will lead to the formation of neutral $[Cr_6Se_8(PEt_3)_6]$,[9] whereas the oxidation of the sulfide-bridged cluster analogue $[Cr_6S_8(H)(PEt_3)_6]$ with $[FeCp_2]BF_4$ is reported to yield ionic $[Cr_6S_8(H)(PEt_3)_6]BF_4$.[29] Furthermore, according to Saito, the Cr···Cr distances for the 'hydrogen-free' $[Cr_6E_8(PEt_3)_6]$ (E = S, Se) are longer by almost 10 pm compared to the cluster putatively incorporating a hydrogen atom, whereas calculations suggest the opposite behaviour, namely an extension of Cr···Cr distances by 5 pm for the inclusion of a hydrogen atom.

Alternatively, the rationalization of the observed extended bond distances and the non-vanishing magnetic moments may arise from our findings of (a) small HOMO–LUMO gaps or low lying excited states with higher multiplicity, respectively, (b) the sensitivity of the Cr···Cr atom distances towards electron addition as well as towards the electronic states and (c) the measured distinct T-dependence of the Cr···Cr atom distance in $[Cr_6E_8(PEt_3)_6]$ (E = S, Se). This means that in $[Cr_6E_8(PEt_3)_6]$ (E = S, Se, Te) even at 2 K the excited spin states ($S = 1$ and/or 2) are populated to a certain extent and increase in relevance with increasing temperature. The dc magnetic data therefore resemble a very broad low spin ($S = 0$) / high spin ($S = 2$) transition (in analogy to a d^6 transition metal complex) which is not complete at both ends of the temperature range (2 K $S \sim \frac{1}{2}$, 300 K $S \geq 1.2$).

For the related molybdenum cluster complexes $[MoE_8(PEt_3)_6]$ (E = S, Se) there exists a good agreement between the Mo···Mo distances calculated for a low spin $S = 0$ ground state and the experimentally determined ones.[18] In line with these findings, the molecules are reported to be diamagnetic.

Experimental section

Synthesis

Standard Schlenk techniques were employed throughout the syntheses using a double manifold vacuum line with high purity dry nitrogen (99.9994%) and an MBraun glovebox with high purity dry argon (99.9990%). The solvents Et$_2$O (diethylether), thf (tetrahydrofuran) and toluene were dried over sodium-benzophenone, and distilled under nitrogen. Anhydrous methylene chloride (CH$_2$Cl$_2$) (H$_2$O <0.005%)

obtained from Sigma-Aldrich was degassed, freshly distilled and stored over molecular sieves under nitrogen. Anhydrous CrCl$_2$ and CrCl$_3$ were obtained from Sigma-Aldrich. $[CrCl_3(thf)_3]$,[36] E(SiMe$_3$)$_2$ (E = S, Se, Te)[37] and PEt$_3$ [38,39] were prepared according to literature procedures. The two latter classes of compounds are toxic, badly smelling, and air and water sensitive compounds which have to be handled with great care according to the respective safety regulations.

$[Cr_6S_8(PEt_3)_8]\cdot1.5C_4H_8O$ (1a). 1 eq. of CrCl$_2$ (82 mg, 0.662 mmol) and 2 eq. of $[CrCl_3(thf)_3]$ (210 mg, 1.324 mmol) were dissolved upon addition of 6 eq. of PEt$_3$ (0.6 mL, 4.02 mmol) in 20 mL of thf. After 15–30 min, a blue solution was formed followed by the addition of 4.2 eq. of S(SiMe$_3$)$_2$ (0.84 mL, 3.972 mmol). After one night of stirring at rt, the reaction solution was heated at 67–74 °C in an oil bath for 6 h to give a dark green solution. After cooling to rt, 5 mL of volatile products were removed by vacuum condensation and again 5 mL of thf was added to the reaction solution. Heating again at 67–74 °C in an oil bath for 6 h afforded a more intensely coloured dark solution with a red shine when inspected with a cold light source. Upon cooling and standing at rt a black crystalline precipitate of **1a** was formed and was separated by decantation and washed three times with 10 mL of cold (0 °C) thf before drying in a vacuum (yield; 200 mg, 44.8%). (**1a**) C$_{42}$H$_{102}$Cr$_6$O$_{1.5}$P$_6$S$_8$ (1385.56): calcd C 36.41, H 7.42, S 18.51 found C 36.96, H 7.33, S 16.23%. Values lower than the calculated values for sulfur might be rationalized by incomplete combustion of the compound and have been detected for several different batches and for recrystallized **1b**.

$[Cr_6S_8(PEt_3)_8]$ (1b). **1a** (250 mg, 0.180 mmol) was dissolved in 25 mL of toluene. In case of remaining undissolved material the solution was once filtered or centrifuged. After layering with Et$_2$O or EtOH black crystals of **1b** were formed over several days. They were separated by decantation and washed three times with Et$_2$O before drying in a vacuum (yield; 140 mg, 61%).

(**1b**) C$_{36}$H$_{90}$Cr$_6$P$_6$S$_8$ (1277.44): calcd C 33.85, H 7.10, S 20.08 found C 33.69, H 6.55, S 17.68.

$[Cr_6Se_8(PEt_3)_8]\cdot1.5C_4H_8O$ (2a). 1 eq. of CrCl$_2$ (82 mg, 0.662 mmol) and 2 eq. of $[CrCl_3(thf)_3]$ (496 mg, 1.324 mmol) were dissolved upon addition of 6 eq. of PEt$_3$ (0.6 mL, 4.02 mmol) in 20 mL of thf. After 15–30 min, a blue solution was formed followed by the addition of 4 eq. of Se(SiMe$_3$)$_2$ (0.6 mL, 2.65 mmol). After six hours of stirring at rt, the reaction solution became dark green in colour and was allowed to stand. Black crystals of **2a** were formed over a few days. They were separated by decantation and washed three times with 10 mL of cold (−70 °C) thf before drying in a vacuum (yield; 390 mg, 65%).

(**2a**) C$_{42}$H$_{102}$Cr$_6$O$_{1.5}$P$_6$Se$_8$ (1760.76): calcd C 28.65, H 5.84 found C 28.95, H 5.92%.

$[Cr_6Se_8(PEt_3)_8]$ (2b). **2a** (250 mg, 0.142 mmol) was dissolved in 25 mL of toluene. In case of remaining undissolved material the solution was once filtered or centrifuged. After layering with Et$_2$O or EtOH black crystals of **2b** were formed over several days. These were separated by decantation and washed

three times with 10 mL of Et_2O before drying in a vacuum (yield; 170 mg, 72.4%).

(**2b**) $C_{36}H_{90}Cr_6P_6Se_8$ (1652.60): calcd C 26.16, H 5.49 found C 26.47, H 5.19%.

[**$Cr_6Te_8(PEt_3)_8$**] (**3**). 1 eq. of $CrCl_2$ (82 mg, 0.662 mmol) and 2 eq. of [$CrCl_3(thf)_3$] (496 mg, 1.324 mmol) were dissolved upon addition of 4 eq. of PEt_3 (0.4 mL, 2.67 mmol) in 15 mL of thf. After 15–30 min, a blue solution was formed and was cooled down to −40 °C in a dry ice/methanol bath followed by the addition of 4 eq. of $Te(SiMe_3)_2$ (0.61 mL, 2.67 mmol). For three hours, the reaction solution was kept in a freezer at −45 °C and then moved to a refrigerator at 0 °C. Black small crystals of **3** were formed over a few days. They were separated by decantation and washed two times with 10 mL of cold (−40 °C) thf/Et_2O (1 : 1) and once with cold (−40 °C) thf/pentane (1 : 1) before drying in a vacuum (yield; 170 mg, 53%).

(**3**) $C_{36}H_{90}Cr_6P_6Te_8$ (2041.18): calcd C 21.65, H 4.44 found C 21.82, H 4.31%.

Crystallography

Due to the air and moisture sensitivity of the compounds, crystals suitable for single crystal X-ray diffraction were selected in perfluoroalkylether oil and mounted quickly on a diffractometer equipped with an Oxford Cryosystem.

Single-crystal X-ray diffraction data of **1a** and **2b** were collected on a STOE IPDS II (Imaging Plate Diffraction System) using graphite-monochromatised MoKα radiation (λ = 0.71073 Å) generated by a sealed X-ray tube, with a 12 × 0.4 mm long-fine focus. Single-crystal X-ray diffraction data of **1b** were collected using MoKα radiation (λ = 0.71073 Å) generated by a microfocus sealed X-ray tube (Mo Genix 3D) with a multilayer optic on a STOE STADI Vari (Pilatus Hybrid Pixel Detector 300 K). Single-crystal X-ray diffraction data of **2a** were collected on a STOE IPDS II (Imaging Plate Diffraction System) using graphite-monochromatised MoKα radiation (λ = 0.71073 Å) generated by a Bruker rotating anode. Single-crystal X-ray diffraction data of **3** were collected on a STOE IPDS II (Imaging Plate Diffraction System) using synchrotron radiation (λ = 0.80 Å) at the ANKA synchrotron source in Karlsruhe.

Temperature dependent single-crystal X-ray diffraction data of **1b** and **2b** were collected using GaKα radiation (λ = 1.34143 Å) generated by a Ga Metaljet D2 with a Montel multilayer optic on a STOE STADI Vari (Dectris Eiger Hybrid Pixel Detector 4M).

Raw intensity data were collected and treated with the STOE X-Area software. Data for all compounds were corrected for Lorentz and polarisation effects.

Based on a crystal description, absorption corrections were applied for **1a**, **2a**, **2b** and **3** by integration.[40] For **1b** interframe scaling of the dataset was performed with the implemented program STOE LANA and a multi-scan absorption correction was applied by scaling of reflection intensities.[41]

Using Olex2,[42] the structures were solved with the ShelXT[43] structure solution program using Intrinsic phasing and refined with the ShelXL [3][44] refinement package using Least squares minimisation.

Molecular diagrams were prepared using Diamond.[45]

In **1–3** all Cr, S, Se, Te, P and C atoms were refined with anisotropic displacement parameters, whilst H atoms were computed and refined using a riding model, with the isotropic temperature factor equal to 1.2 times the equivalent temperature factor of the atom to which they are linked. Lattice solvent molecules were identified within the structures of **1a** and **2a**. They were located at special positions and could not be adequately refined due to disorder. Therefore, for correction, the solvent masking routine implemented in Olex2 was used, based on the method described by van der Sluis and Spek.[46] The following corrections were applied:

1a a total of 327 electrons in a potential solvent accessible area of ~1026 $Å^3$ (~4.5 C_4H_8O).

2a a total of 281 electrons in a potential solvent accessible area of ~1031.7 $Å^3$ (~3.9 C_4H_8O).

CCDC 2172332 (**1a**), 2172333 (**1b**), 2172334 (**2a**), 2172336 (**2b**) and 2172335 (**3**) contain the supplementary crystallographic data for this paper.†

X-ray powder diffraction patterns (XRD) for **1–3** (powder of crystals) were measured at rt on a STOE STADI P diffractometer (Cu-K$_{\alpha1}$ radiation, germanium primary monochromator, Debye–Scherrer geometry, Mythen 1 K detector) in sealed glass capillaries. The theoretical powder diffraction patterns were calculated on the basis of the atom coordinates obtained from single crystal X-ray analysis (180 K) by using the program package STOE WinXPOW.[47]

Temperature dependent XRD powder patterns of **3** were measured on a STOE STADI P diffractometer (Ag K$_{\alpha1}$ radiation, germanium 111 primary monochromator, Debye–Scherrer geometry, and Mythen 1K detector) in sealed glass capillaries.

Physical measurements

C, H, and S elemental analyses were performed on an Elementar vario Micro cube instrument.

UV-Vis absorption spectra of **1–3** in C_6D_6 were measured on a PerkinElmer Lambda 900 spectrophotometer in quartz cuvettes.

Thermogravimetric analyses were performed in Al_2O_3 crucibles on a thermobalance STA 409 from Netzsch in a dynamic helium gas flow (25 ml min^{-1}) and under vacuum conditions 1.5×10^{-6} mbar at a heating rate of 2 °C min^{-1}. The crucibles were filled (20–35 mg) inside an argon glove box, transferred into Schlenk tubes and mounted under a stream of argon to the balance. Caution should be taken with respect to the bad smelling volatile products formed in the TGA.

Mass spectra were recorded on a Bruker Micro TOF Q2 instrument equipped with an ESI NanoSource.

Zero-Field-Cooled (ZFC) temperature dependent susceptibilities were recorded for **1a**, **2a**, **1b**, **2b** and **3** in dc mode using a MPMS-III (Quantum Design) SQUID magnetometer over a temperature range from 2 to 300 K in a homogeneous 0.1 T external magnetic field. The magnetization curves were measured on the same instrument up to a dc field of 7 T.

Ac susceptibility measurements of **1a**, **2a**, **1b**, **2b** and **3** were performed at 2 K using an MPMS-XL (Quantum Design) SQUID

magnetometer with an oscillating ac field of 3 Oe and at ac frequencies ranging from 1 to 1500 Hz. There is no indication of a relevant signal of the out-of-phase component of the ac susceptibility (χ'') even under applied dc fields up to 2500 Oe which indicates that under these conditions the spin lattice relaxation is faster than the timescale of the experiment.

The samples were mixed with icosane and compressed in gelatine capsules in a glove box under an argon atmosphere owing to the high degree of moisture and oxygen sensitivity of the compounds. The samples were transferred into sealed Schlenk tubes from the glove box to the magnetometer and then rapidly transferred to the helium-purged sample space of the magnetometer. The data were corrected for the sample holder including the gelatine capsule, and for the diamagnetism of icosane and the sample itself using Pascal's constants.[48–50]

We note that repetitive magnetic measurements lead especially for the solvent containing samples **1a** and **2a** to slightly varying curves. Beside a possible change in the solvent content upon storage in a glove box under argon other main factors for this behaviour can be balancing errors in the glovebox and/or slight reactions of the reactive cluster complexes with the walls of the gelatin capsules.

EPR measurements

EPR measurements at the X-band (9.4 GHz) were carried out using a Bruker ELEXSYS E580 CW EPR spectrometer equipped with an Oxford Instruments helium cryostat (ESR900) and a MercuryiTC temperature controller.

Quantum chemical calculations

Density functional calculations were performed with TURBOMOLE,[51,52] employing functionals PBE[53–56] PBE0[53,54–57] and B3LYP,[53,54,58–60] along with polarized triple-zeta valence basis sets def2-TZVP,[61] within the RI-J approximation[62] throughout. Electronic excitations were calculated using TDDFT.[63] Atomic contributions to molecular orbitals were obtained from Mulliken population analyses.[64] The character of the electronic excitation bands was visualized using the non-relaxed transition densities as described previously.[65]

Author contributions

A. E. was responsible for synthesis and characterization, P. B. and F. W. for DFT and TDDFT calculations and I. K. for EPR spectroscopy.

Conflicts of interest

The authors declare no financial interests.

Acknowledgements

References

1 *Clusters and Colloids: From theory to applications*, ed. G. Schmid, VCH, Weinheim, 1994.

2 *Metal Clusters in Chemistry*, ed. P. Braunstein, L. A. Oro and P. R. Raithby, Wiley-VCH Verlag GmbH, Weinheim, 1999, vol. I–III.

3 S. C. Lee and R. H. Holm, *Angew. Chem., Int. Ed. Engl.*, 1990, **29**, 840–856.

4 I. Dance and K. Fisher, *Progress in Inorganic Chemistry*, ed. K. D. Karlin, John Wiley & Sons, Inc., New York, Weinheim, 1994, vol. 41, pp. 637–802.

5 O. Fuhr, S. Dehnen and D. Fenske, *Chem. Soc. Rev.*, 2013, **42**, 1871–1906.

6 M. W. DeGroot and J. F. Corrigan, in *The Chemistry of nanomaterials: Synthesis, properties and applications*, ed. C. N. R. Rao, A. Mueller and A. K. Cheetham, Wiley-VCH, 2004, pp. 418–451.

7 K. Tsuge, H. Imoto and T. Saito, *Bull. Chem. Soc. Jpn.*, 1996, **69**, 627–636.

8 B. Hessen, T. Siegrist, T. Palstra, S. M. Tanzler and M. L. Steigerwald, *Inorg. Chem.*, 1993, **32**, 5165–5169.

9 S. Kamiguchi, H. Imoto and T. Saito, *Inorg. Chem.*, 1998, **37**, 6852–6857.

10 D. Fenske, J. Ohmer and J. Hachgenei, *Angew. Chem., Int. Ed. Engl.*, 1985, **24**, 993–995.

11 M. L. Steigerwald, T. Siegrist and S. M. Stuczynski, *Inorg. Chem.*, 1991, **30**, 2256–2257.

12 M. L. Steigerwald, T. Siegrist and S. M. Stuczynski, *Inorg. Chem.*, 1991, **30**, 4940–4945.

13 B. Choi, B. Capozzi, S. Ahan, A. Turkiewicz, G. Lovat, C. Nuckolls, M. L. Steigerwald, L. Venkataraman and X. Roy, *Chem. Sci.*, 2016, **7**, 2701–2705.

14 X. Roy, C.-H. Lee, A. C. Crowther, C. L. Schenck, T. Besara, R. A. Lalancette, T. Siegrist, P. W. Stephens, L. E. Brus, P. Kim, M. L. Steigerwald and C. Nuckolls, *Science*, 2013, **341**, 157–160.

15 B. Choi, J. Yu, D. W. Paley, M. Tuan-Trinh, M. V. Paley, J. M. Karch, A. C. Crowther, C.-H. Lee, R. A. Lalancette, X. Zhu, P. Kim, M. L. Steigerwald, C. Nuckolls and X. Roy, *Nano Lett.*, 2016, **16**, 1445–1449.

16 J. Yang, J. C. Russell, S. Tan, M. Lessin, F. Wang, A. C. Hartnett, S. R. Peurifoy, E. A. Doud, E. S. O'Brien, N. Gadjieva, D. R. Reichman, X. Zhu, A. C. Crowther, S. J. L. Billinger, X. Roy, M. L. Steigerwald and C. Nuckolls, *Nat. Chem.*, 2021, **13**, 607–613.

17 F. S. Delk and M. J. Sienko, *Inorg. Chem.*, 1980, **19**, 1352; M. Potel, R. Chevrel and M. Sergent, *Acta Crystallogr., Sect. B: Struct. Crystallogr. Cryst. Chem.*, 1980, **36**, 1319.

18 P.-D. Fan, P. Deglmann and R. Ahlrichs, *Chem. – Eur. J.*, 2002, **8**, 1059–1067.

19 A. Bencini, S. Midollini and C. Zanchini, *Inorg. Chem.*, 1992, **31**, 2132–2137.

20 F. Cecconi, C. A. Ghilardi, S. Midollini and A. Orlandini, *Inorg. Chim. Acta*, 1983, **76**, L183–L184.

21 F. Cecconi, C. A. Ghilardi, S. Midollini and A. Orlandini, *Polyhedron*, 1986, **5**, 2021–2031.

22 A. Bencini, C. A. Ghilardi, S. Midollini, A. Orlandini and C. Zanchini, *J. Am. Chem. Soc.*, 1992, **114**, 9898–9908.

23 C. A. Goddard, J. R. Long and R. H. Holm, *Inorg. Chem.*, 1996, **35**, 4347–4354.

24 A. Bencini, C. A. Ghilard, S. Midollini, A. Orlandini, U. Russo, M. G. Uytterhoevena and C. Zanchini, *J. Chem. Soc., Dalton Trans.*, 1995, 963–974.

25 S. M. Stuczynski, J. G. Brennan and M. L. Steigerwald, *Inorg. Chem.*, 1989, **28**, 4431–4432.

26 J. F. Corrigan, O. Fuhr and D. Fenske, *Adv. Mater.*, 2009, **21**, 1867–1871.

27 S. Dehnen, A. Eichhöfer and D. Fenske, *Eur. J. Inorg. Chem.*, 2002, 279–317.

28 D. Fenske, J. Ohmer, J. Hachgenei and K. Merzweiler, *Angew. Chem., Int. Ed. Engl.*, 1988, **27**, 1277–1296.

29 S. Kamiguchi, T. Saito and Z. Honda, *Organomet. Chem.*, 2000, **609**, 184–188.

30 T. Saito, N. Yamamoto, T. Yamagata and H. Imoto, *J. Am. Chem. Soc.*, 1988, **110**, 1646–1647.

31 T. Saito, N. Yamamoto, T. Nagase, T. Tsuboi, K. Kobayashi, T. Yamagata, H. Imoto and K. Unoura, *Inorg. Chem.*, 1990, **29**, 764–770.

32 J. D. Satterlee, *Concepts Magn. Reson.*, 1990, **2**, 119–129.

33 R. P. Bonomo, A. J. Di Bilio and R. Riggi, *Chem. Phys.*, 1991, **151**, 323–333.

34 M. B. Robin and P. Day, *Adv. Inorg. Chem. Radiochem.*, 1967, **10**, 247.

35 G. J. Ribas, *Coordination Chemistry*, Wiley-VCH Verlag GmbH & Co, KGaA, Weinheim, 2008, ch. 13, p. 403.

36 B. Heyn, B. Hipler, G. Kreisel, H. Schreer and D. Walther, *Anorganische Synthesechemie: ein integriertes Praktikum*, Springer-Verlag Berlin, Heidelberg, New York, 1986, p. 23.

37 H. Schmidt and H. Ruf, *Z. Anorg. Allg. Chem.*, 1963, **321**, 270–273.

38 K. Sasse, in *Methoden der Organischen Chemie, Band 1*, ed. J. Houben and T. Weyl, Thieme Verlag, Stuttgart, 1963, p. 32.

39 H. D. Kaesz and F. G. Stone, *J. Org. Chem.*, 1959, **24**, 635–637.

40 STOE X-Red32, absorption correction by Gaussian integration, analogous to P. Coppens, The Evaluation of Absorption and Extinction in Single-Crystal Structure Analysis, ed. F. R. Ahmed, *Crystallographic Computing*, Munksgaard, Copenhagen, 1970, pp. 255–270.

41 STOE LANA, absorption correction by scaling of reflection intensities. J. Koziskova, F. Hahn, J. Richter and J. Kozisek, Comparison of different absorption corrections on the model structure of tetrakis(\m~2~-acetato)-diaqua-di-copper (ɪɪ), *Acta Chimica Slovaca*, 2016, vol. 9, no. 2, pp. 136–140.

42 O. V. Dolomanov, L. J. Bourhis, R. J. Gildea, J. A. K. Howard and H. Puschmann, *J. Appl. Crystallogr.*, 2009, **42**, 339–341.

43 G. M. Sheldrick, *Acta Crystallogr., Sect. A: Found. Adv.*, 2015, **71**, 3–8.

44 G. M. Sheldrick, *Acta Crystallogr., Sect. C: Struct. Chem.*, 2015, **71**, 3–8.

45 K. Brandenburg, *Diamond Version 2.1d, Crystal Impact GbR*, 1996–2000.

46 A. L. Spek, *Acta Crystallogr., Sect. A: Found. Crystallogr.*, 1990, **46**, C-34.

47 *STOE, WinXPOW*, STOE & Cie GmbH, Darmstadt, 2000.

48 O. Kahn, *Molecular Magnetism*, Wiley-VCH, Weinheim, 1993.

49 H. Lueken, *Magnetochemie*, B. G. Teubner, Stuttgart, Leibzig, 1999, p. 426.

50 W. Haberditzl, *Angew. Chem.*, 1966, **78**, 277–312, (*Angew. Chem. Int. Ed. Engl.*, 1966, **5**, 288–323).

51 TURBOMOLE Version 7.4, TURBOMOLE GmbH 2019. TURBOMOLE is a development of the University of Karlsruhe and the Forschungszentrum Karlsruhe 1989–2007, TURBOMOLE GmbH since 2007.

52 F. Furche, R. Ahlrichs, C. Hättig, W. Klopper, M. Sierka and F. Weigend, Turbomole, *Wiley Interdiscip. Rev.: Comput. Mol. Sci.*, 2014, **4**, 91–100.

53 P. A. M. Dirac and R. H. Fowler, *Proc. R. Soc. London, Ser. A*, 1929, **123**, 714–733.

54 J. C. Slater, *Phys. Rev.*, 1951, **81**, 385–390.

55 J. P. Perdew and Y. Wang, *Phys. Rev. B: Condens. Matter Mater. Phys.*, 1992, **45**, 13244–13249.

56 J. P. Perdew, K. Burke and M. Ernzerhof, *Phys. Rev. Lett.*, 1996, **77**, 3865–3868.

57 J. P. Perdew, M. Ernzerhof and K. Burke, *J. Chem. Phys.*, 1996, **105**, 9982–9985.

58 C. Lee, W. Yang and R. G. Parr, *Phys. Rev. B: Condens. Matter Mater. Phys.*, 1988, **37**, 785–789.

59 A. D. Becke, *Chem. Phys.*, 1993, **98**, 5648–5652.

60 A. D. Becke, *Phys. Rev. A*, 1988, **38**, 3098–3100.

61 F. Weigend and R. Ahlrichs, *Phys. Chem. Chem. Phys.*, 2005, **7**, 3297–3305.

62 F. Weigend, *Phys. Chem. Chem. Phys.*, 2006, **8**, 1057–1065.

63 R. Bauernschmitt and R. Ahlrichs, *Chem. Phys. Lett.*, 1996, **25**, 454–464.

64 R. S. Mulliken, *J. Chem. Phys.*, 1955, **23**, 1833–1840.

65 M. Kühn and F. Weigend, *J. Chem. Phys.*, 2014, **141**, 22302.